
Article:
Yang, Long, Yan, Yu, Chen, Yequan et al. (9 more authors) (2020) Large anisotropy of magnetic damping in ultrathin epitaxial Fe/GaAs (001) film. Journal of Physics D: Applied Physics. 115004. ISSN 0022-3727

https://doi.org/10.1088/1361-6463/ab61cd

Large anisotropy of magnetic damping in ultrathin epitaxial Fe/GaAs (001) film

Long Yang,[1] Yu Yan,[1,2] Yequan Chen,[1] Yiyi Chen,[1] Bo Liu,[1] Zhendong Chen,[1] Xianyang Lu,[1] Jing Wu,[2] Liang He,[1] Xuezhong Ruan,[1,a)] Bo Liu,[3] and Yongbing Xu[1,2,a)]

[1]*Jiangsu Provincial Key Laboratory of Advanced Photonic and Electronic Materials, School of Electronic Science and Engineering, Nanjing University, Nanjing 210093, P. R. China.*

[2]*York-Nanjing International Center in Spintronics, Department of Electronic Engineering and Department of Physics, The University of York, York YO10 5DD, UK.*

[3]*Zhejiang Hikstor Technology CO., LTD, Hangzhou 311300, People's Republic of China.*

Abstract

The magnetization dynamics of ultrathin epitaxial Fe films on GaAs (001) with different thicknesses have been investigated by all-optical time-resolved magneto-optical Kerr effect. For the Fe film with thickness of 8 monolayers, the magnetic damping constants show a large uniaxial anisotropy with an increase of up to 66% depending on the crystallographic directions. The uniaxial magnetic damping correlates clearly with the in-plane uniaxial anisotropy field obtained by fitting the dispersion equation. In addition, the anisotropy of the damping constants is found to disappear for the Fe films thicker than 15 monolayers, suggesting that the anisotropic damping originates from the interfacial effect between Fe and GaAs.

Index Terms—Anisotropic damping constant, ultrathin film, TR-MOKE, magnetic anisotropy field.

[a)]Author to whom correspondence should be addressed. Electronic mails: xzruan@nju.edu.cn and ybxu@nju.edu.cn

Magnetic damping constant plays a key role in magnetic procession and spin relaxation process in magnetization dynamics.[1-3] It is one of the key issues for spintronic applications as well. A typical example is magnetic random access memory (MRAM), in which the critical current density to switch the magnetization is proportional to the magnetic damping constant. To reduce the critical current of the STT-MRAM, a magnetic material with small damping constant should be considered. However, a magnetic material with small damping constant increases spin switching time, and thus reduces the operating speed. [4, 5] Therefore, it is of great importance to find a magnetic material with proper damping constant. In order to investigate the physical mechanisms of magnetic damping, a few works have been done in recent years.[6-13] These reports reveal that several factors have impact on the magnetic damping constant, such as the thickness,[6] the capping layer,[7, 8] and the magnetic anisotropy of the film.[9, 10] In addition, external electric field and pulsed laser can also change the damping constant.[11-13] Theoretically, the intrinsic magnetic damping is proportional to ξ^2/τ, where ξ is the strength of the spin–orbit interaction and τ is the electron momentum scattering time.[14, 15] Generally, the magnetic damping constant is regarded as an isotropic constant irrelevant to the crystal directions.

At the same time, the Fe/GaAs (001) hybrid structure has been one of the interesting topics.[16-19] Over the last decades, It is a model hybrid ferromagnetic (FM)/semiconductor (SC) system due to the fact that the lattice mismatch is reasonably low (~1.4%), providing a basis for epitaxial growth.[18] In addition, the respective properties of Fe film and GaAs are widely studied, because Fe is a robust FM material with high spin polarization while GaAs is the most commonly used III-V SC in device applications. The interface between Fe and GaAs induces uniaxial magnetic anisotropy for ultrathin Fe film, which is different from the cubic magnetic anisotropy induced by the crystal structure of Fe film.[20] Several reports have indicated that the magnetic damping constant is anisotropic in monocrystalline Fe film.[21-23] Recently, L. Chen et al. reported an anisotropic damping constant with an increase of around 20% in Fe film measured by spin-orbit ferromagnetic resonance (SO-FMR).[19] Here, we investigate the anisotropy of the damping constant in the Fe/GaAs system with various thicknesses of Fe layer. The anisotropic damping constant was measured by angular dependent time-resolved magneto-optical Kerr effect (TR-MOKE). Comparing the damping constant along $[\bar{1}10]$ orientation with that along [110] orientation, we find a large increase of up to 66% in the Fe film with the thickness of 8 monolayers (MLs). Such an anisotropy

of damping constant is in accordance with the in-plane uniaxial anisotropy of the film and thus we deduce that the anisotropy of damping constant originates from interfacial effect between Fe and GaAs.

The bilayer Cr(3 nm)/Fe(t) films were deposited on commercially available GaAs (001) substrates by molecular beam epitaxy (MBE). The thickness of Fe films was selected as t = 8, 15, 20, 24, 32, 40 MLs. To protect the Fe layer from oxidization, a 3 nm Cr capping layer was deposited on the top of Fe layer. The base pressure of the chamber was below 2×10^{-10} mbar while the Fe and Cr growth pressure were 6×10^{-10} mbar and 1×10^{-9} mbar, respectively. During the deposition, the lattice structure of the deposited layers was monitored by a reflective high energy electron diffraction (RHEED) to insure high quality of monocrystalline Fe film.

The static magnetic property of monocrystalline Fe film was measured by a vibrating sample magnetometer (VSM), where the external magnetic field was applied in the film plane. In Fig. 1(a), the in-plane hysteresis loops of 8 MLs Fe are depicted. The coercivity of 8 MLs Fe is around 12.5 Oe along $[110]$ orientation of the GaAs substrate while it is about 50.1 Oe along $[\bar{1}10]$ orientation. The saturation magnetization $\underline{M_s}$ is around 2000 emu/cm^3. Magnetization dynamics were investigated by means of all-optical TR-MOKE. Fig. 1(b) illustrates the schematic configuration of the polar TR-MOKE measurement and the coordinate system used for analysis. The surface normal of Fe film is defined as z-axis. The pump beam is incident along negative z-axis while the incident probe beam is about 4° away from z-axis. The spot diameters of pump and probe beams focused onto the film surface are about 500 μm and 200 μm, respectively. $\vec{H}_{ext}$ is applied obliquely to pull the magnetization of Fe film out of the sample plane. The effective magnetic field $\vec{H}_{eff}$ is a vector field composed of the external magnetic field $\vec{H}_{ext}$ and the magnetic anisotropy field (MAF) of the film. θ_H (θ) is the polar angel and φ_H (φ) is the azimuthal angel of $\vec{H}_{ext}$ ($\vec{H}_{eff}$). Once pump pulse beam is incident on the sample surface, energy deposited by the pump pulse leads to a change of the MAF and thus $\vec{H}_{eff}$. A transiently induced $\vec{H}_{eff}{}'$ deviates from the original equilibrium $\vec{H}_{eff}$ and recovers to $\vec{H}_{eff}$ within about 10 picoseconds.[24] Consequently, the magnetization $\vec{M}$ is triggered out of equilibrium by $\vec{H}_{eff}{}'$ and starts to relax by damped oscillation around $\vec{H}_{eff}$. Generally, the precessional motion detected by probe beam lasts up to the nanosecond scale.[25, 26] In the TR-MOKE measurements, the femtosecond pulse laser is generated by

a Ti:sapphire regenerative amplifier with a repetition rate of 1 kHz, a central wavelength of 800 nm, and pulse duration of about 60 fs, respectively. The pump beam fluence is 15.3 mJ/cm^2. All measurements were performed with an fixed angle $\theta_H = 60°$ at room temperature. The details of the TR-MOKE setup were also described in the previous reports.[9, 27]

The sample is placed in XY-plane with [110] orientation pointing to positive x-axis as shown in Fig. 1(b). The component of $\vec{H}_{ext}$ projected on XY-plane is along $[110]$ or $[\bar{1}10]$ orientations when φ_H is 0° or 90° respectively. For TR-MOKE measurement, the damped oscillation curves can be described by the following phenomenological formula:[1, 28]

$$\theta_{Kerr} \propto Ae^{-t/\tau} sin(2\pi ft + \varphi_0) + Be^{-t/\tau_1} \quad (1)$$

where A, τ, f, and φ_0 are the amplitude, relaxation time, frequency and initial phase of the magnetization precession, respectively. The second term of Eq. (1) represents the background signal due to the demagnetization recovery.[9, 14] Fig. 2(a) shows the typical TR-MOKE signal of 8 MLs Fe film measured along $[\bar{1}10]$ orientation. The damped oscillating signals excited by pump laser correspond to the strong magnetization precession. The external magnetic fields are varied from 1.191 kOe to 6.858 kOe. The red solid curves are the best fitting results, suggesting that the optically excited procession of magnetization is a uniform mode. Fig. 2(b) displays the precessional frequencies f as a function of external field along $[110]$ and $[\bar{1}10]$ orientations, showing different trend along these two orthogonal orientations. f is almost linear to external field along $[110]$ orientation, indicating that the effective magnetic field is mainly contributed by the external magnetic field. However, f behaves nonlinearly with the magnetic field along $[110]$ orientation, especially in the low field region, suggesting a high MAF along this orientation. The solid curves in Fig. 2(b) are the calculated results of frequency, and the formula is expressed as:[29]

$$\left(\frac{2\pi f}{\gamma}\right)^2 - \frac{1}{M_S^2 sin^2\theta}\left[\frac{\partial^2 F}{\partial\theta^2}\frac{\partial^2 F}{\partial\varphi^2} - \left(\frac{\partial^2 F}{\partial\theta\partial\varphi}\right)^2\right] = 0 \quad (2)$$

where M_s is the saturation magnetization and F is the magnetic energy density. γ is the gyromagnetic ratio and it is defined as $\gamma \equiv g\mu_B/\hbar$ where g, μ_B, and $\hbar$ are the Lande's g-factor, Bohr magneton, and the reduced Planck's constant, respectively. g is taken as 2.1 for Fe film in general. The in-plane magnetic anisotropy of ultrathin Fe film is cubic anisotropy superimposed with uniaxial anisotropy, thus the total energy density F is modeled by:[29]

$$F = -M_s H[sin\theta sin\theta_H cos(\varphi - \varphi_H) + cos\theta cos\theta_H] - (2\pi M_s^2 - K_\perp)sin\theta^2 + K_u sin^2\theta cos^2\varphi$$
$$-1/8K_c[3 + cos4(\varphi - \varphi_0)]sin^4\theta \quad (3)$$

where K_u, K_c, and $K_\perp$ are in-plane uniaxial, cubic, and perpendicular anisotropy constants, respectively. The four terms in Eq. (3) represent Zeeman energy, the effective demagnetization energy, the in-plane uniaxial anisotropy energy, and in-plane cubic anisotropy energy, successively. φ_0 is the initial phase of cubic anisotropy with respect to the positive x-axis, i.e., the easy axis of the uniaxial anisotropy. θ and φ are determined by the minimum of F by using the conditions $\partial F/\partial\theta = 0$ and $\partial F/\partial\varphi = 0$ when effective field is in the equilibrium state. Combining with Eqs. (2)-(3), we obtain the ultimate fitting formula as shown in Eq. S1. Then, the fitting frequency values are calculated by the best fitting parameters K_u, K_c and $K_\perp$ according to Eq. (S1). The effective demagnetization field $4\pi M_{eff}$ is calculated by $4\pi M_{eff} = 4\pi M_s - 2K_\perp / M_s$. In terms of the fitting parameter $K_\perp$, we obtain $4\pi M_{eff[110]} = 7.29 \pm 1.27$ kOe and $4\pi M_{eff[\bar{1}10]} = 5.13 \pm 2.38$ kOe. Generally, the effective demagnetization field is a constant for in-plane magnetized film. However, the calculated values of $4\pi M_{eff}$ along $[110]$ and $[\bar{1}10]$ are not equivalent due to large fitting error, and we will discuss this later on. Fig. 2(c) shows the effective damping factor α_{eff} under different magnetic fields, in which α_{eff} is given by $\alpha_{eff} = 1 / (2\pi f\tau)$. The intrinsic damping factor α_0 is regarded as a constant due to the natural property of magnetic material. Theoretically, α_0 is an ultimate value of α_{eff} as the external field approaches to an infinity, and thus it can be extracted approximately at a high field.[30-32] As shown in Fig. 2(c) of the 8MLs film, the effective damping factor decreases dramatically with increasing the external field and eventually keeps unchanged. The invariable α_{eff} is approximately regarded as intrinsic damping α_0 and thus we extracted average α_0 along two orthogonal orientations from external field exceeding 5.5 kOe. The results are $\alpha_{0[110]} = 0.0123 \pm 0.0015$ and $\alpha_{0[\bar{1}10]} = 0.0204 \pm 0.0023$. The intrinsic damping constant along $[\bar{1}10]$ orientation increases by 66% compared with that along $[110]$ orientation, indicating that the intrinsic damping constant is not isotropic in the ultrathin Fe film.

To further investigate the anisotropy of damping constant of 8MLs Fe film, the angular dependent TR-MOKE was performed by changing the angle φ_H of the crystallographic orientation of GaAs with respect to $\vec{H}_{ext}$. More specifically, φ_H is changed from 0° to 360° with step of 10°. The value of external magnetic field was set as 6.24 kOe to obtain intrinsic damping constant. Fig. 3(a)-(c) provide the decay

time, frequency, and intrinsic damping constant according to Kerr signals measured by rotating the sample in the XY-plane. The precessional frequencies show a clear two-fold symmetry and the symmetrical axes are in accordance with the easy and hard axes of Fe film, indicating a high in-plane MAF. The decay time also presents two-fold symmetry, yet the symmetrical axes tilt around 15°, leading to a similar oblique two-fold symmetry of intrinsic damping constant. The round angular measurements of the TR-MOKE enable us to determine unambiguously the uniaxial and cubic components of the in-plane MAF. In Fig. 3(b), the calculated frequencies are perfectly fitted to the experimental data by adjusting the value of K_u, K_c and $K_\perp$ according to Eq. (S1).

The angular dependent TR-MOKE was also performed for the Fe films with various thicknesses and the angular dependent precessional frequencies are shown in Fig. S1. Subsequently, the MAF is calculated by the best fitting parameters K_u, K_c, and $K_\perp$. The results are plotted in Fig. 4(a), which gives a clear competitive picture between magnetic uniaxial field $2K_u/M_s$ and magnetic cubic field $2K_c/M_s$. For the ultrathin Fe films, the magnetic uniaxial field dominates the in-plane magnetic anisotropy. With the increase of the thickness of the Fe films, the magnetic uniaxial field decreases dramatically and the magnetic cubic field increases until a saturated value. The effective demagnetization field behaves similarly to the cubic field, because both of them are contributed by the bulk state. For Fe film with the thickness of 8 MLs, we would like to point out that the $4\pi M_{eff}$ obtained from fitting f vs φ is 7.23 ± 0.11 kOe. However, $4\pi M_{eff[110]} = 7.29 \pm 1.27$ kOe and $4\pi M_{eff[\bar{1}10]} = 5.13 \pm 2.38$ kOe are calculated by fitting f vs H (φ_H= 0°, 90°). In fact, the effective demagnetization is a constant for in-plane magnetized film. Obviously, 7.23 ± 0.11 kOe is more accurate for the effective magnetization field. For the ultrathin Fe films, the in-plane MAF is the same magnitude as the external magnetic field. Therefore, the system is overdetermined in the low external field region and thus fitting f vs H induces large experimental uncertainties. Fig. 4(b) presents the intrinsic damping constants along $[110]$ and $[\bar{1}10]$ orientations for the Fe films with various thicknesses. The intrinsic damping shows a similar behavior to the magnetic uniaxial with the increase of the thickness of the Fe films. Therefore, we deduce that uniaxial magnetic damping correlates with the in-plane uniaxial anisotropy field. In addition, S. Pal et al also reported that the damping constant is a linear relation with the perpendicular magnetic anisotropy for out-of-plane magnetized $[Co/Pd]_8$, which is in accordance with our results. From the perspective of

electron structure, G. Keith et al reported that the intra-band contribution of Fe film contributed to the directional anisotropy of the scattering rates by the ab initio density functional electron theory.[23] The interface between ultrathin Fe and GaAs exists strong interfacial spin-orbit coupling.[17] Therefore, we deduce that interfacial spin-orbit coupling enhanced the intra-band contribution of Fe film, leading to larger anisotropy of the scattering rates and thus anisotropy of the intrinsic damping constant.

In conclusion, the magnetic damping constants of Fe/GaAs films were studied by TR-MOKE. We find a large uniaxial anisotropy of the damping constant in ultrathin Fe film. The intrinsic damping constant along $[\bar{1}10]$ orientation increases by 66% compared with that along $[110]$ orientation. However, such a uniaxial anisotropy of the damping constant nearly disappears when the Fe films are thicker than 15 MLs, indicating that the anisotropy of damping constant originates from interfacial effect between Fe and GaAs. The large anisotropy of the damping constant in ultrathin Fe films may be beneficial to design the spintronic devices such as spin-orbit torque MRAM and nano-oscillators.

See supplementary material for: I. The ultimate fitting formula of the dispersion relation. II. The precessional frequencies measured by angular TR-MOKE for Fe film with various thicknesses.

Acknowledgement

This work is supported by National Key Research and Development Program of China (Grant No. 2016YFA0300803), the National Natural Science Foundation of China (Grant No. 61427812 and No. 11774160), and the Fundamental Research Funds for the Central Universities (Grant No. 021014380113).

Reference

1. Z. Chen, M. Yi, M. Chen, S. Li, S. Zhou and T. Lai, Applied Physics Letters **101** (22), 222402 (2012).
2. G. Woltersdorf, M. Buess, B. Heinrich and C. H. Back, Phys Rev Lett **95** (3), 037401 (2005).
3. B. Zhang, A. Cao, J. Qiao, M. Tang, K. Cao, X. Zhao, S. Eimer, Z. Si, N. Lei, Z. Wang, X. Lin, Z. Zhang, M. Wu and W. Zhao, Applied Physics Letters **110** (1), 012405 (2017).
4. S. Ikeda, K. Miura, H. Yamamoto, K. Mizunuma, H. D. Gan, M. Endo, S. Kanai, J. Hayakawa, F. Matsukura and H. Ohno, Nat Mater **9** (9), 721-724 (2010).
5. J. C. Slonczewski, Journal of Magnetism and Magnetic Materials **159** (1), L1-L7 (1996).
6. S. Mizukami, E. P. Sajitha, D. Watanabe, F. Wu, T. Miyazaki, H. Naganuma, M. Oogane and Y.

Ando, Applied Physics Letters **96** (15), 152502 (2010).
7. S. Azzawi, A. Ganguly, M. Tokaç, R. M. Rowan-Robinson, J. Sinha, A. T. Hindmarch, A. Barman and D. Atkinson, Physical Review B **93** (5) (2016).
8. A. Natarajarathinam, Z. R. Tadisina, T. Mewes, S. Watts, E. Chen and S. Gupta, Journal of Applied Physics **112** (5), 053909 (2012).
9. B. Liu, L. Yang, X. Z. Ruan, J. W. Cai, L. He, H. Meng, J. Wu and Y. B. Xu, New Journal of Physics **21** (2019).
10. S. Pal, B. Rana, O. Hellwig, T. Thomson and A. Barman, Applied Physics Letters **98** (8), 082501 (2011).
11. A. Okada, S. Kanai, M. Yamanouchi, S. Ikeda, F. Matsukura and H. Ohno, Applied Physics Letters **105** (5), 052415 (2014).
12. Y. Sasaki, K. Suzuki, A. Sugihara, A. Kamimaki, S. Iihama, Y. Ando and S. Mizukami, Applied Physics Express **10** (2), 023002 (2017).
13. B. Liu, X. Ruan, Z. Wu, H. Tu, J. Du, J. Wu, X. Lu, L. He, R. Zhang and Y. Xu, Applied Physics Letters **109** (4), 042401 (2016).
14. P. He, X. Ma, J. W. Zhang, H. B. Zhao, G. Lupke, Z. Shi and S. M. Zhou, Phys Rev Lett **110** (7), 077203 (2013).
15. Y. Liu, A. A. Starikov, Z. Yuan and P. J. Kelly, Physical Review B **84** (1) (2011).
16. S. Qiao, J. Liu, G. Yan, J. Zhao, X. Zhang, S. Wang and G. Fu, Applied Physics Letters **107** (18), 182402 (2015).
17. M. Buchner, P. Hogl, S. Putz, M. Gmitra, S. Gunther, M. A. Schoen, M. Kronseder, D. Schuh, D. Bougeard, J. Fabian and C. H. Back, Phys Rev Lett **117** (15), 157202 (2016).
18. L. Chen, M. Decker, M. Kronseder, R. Islinger, M. Gmitra, D. Schuh, D. Bougeard, J. Fabian, D. Weiss and C. H. Back, Nat Commun **7**, 13802 (2016).
19. L. Chen, S. Mankovsky, S. Wimmer, M. A. W. Schoen, H. S. Körner, M. Kronseder, D. Schuh, D. Bougeard, H. Ebert, D. Weiss and C. H. Back, Nature Physics (2018).
20. L. Sun, P. K. J. Wong, D. X. Niu, X. Zou, Y. Zhai, J. Wu, Y. B. Xu and H. R. Zhai, Journal of Applied Physics **109** (7), 07B910 (2011).
21. Y. Zhai, C. Ni, Y. Xu, Y. B. Xu, J. Wu, H. X. Lu and H. R. Zhai, Journal of Applied Physics **101** (9), 09D120 (2007).
22. Y. Kasatani and Y. Nozaki, Journal of the Magnetics Society of Japan **39** (6), 6 (2015).
23. K. Gilmore, M. D. Stiles, J. Seib, D. Steiauf and M. Fähnle, Physical Review B **81** (17) (2010).
24. J. Walowski, M. D. Kaufmann, B. Lenk, C. Hamann, J. McCord and M. Münzenberg, Journal of Physics D: Applied Physics **41** (16), 164016 (2008).
25. C. Berk, F. Ganss, M. Jaris, M. Albrecht and H. Schmidt, Applied Physics Letters **112** (5), 052401 (2018).
26. M. Van Kampen, C. Jozsa, J. T. Kohlhepp, P. LeClair, L. Lagae, W. J. De Jonge and B. Koopmans, Phys Rev Lett **88** (22), 227201 (2002).
27. Z. Chen, X. Ruan, B. Liu, L. Yang, J. Wu, C. Gao, H. Meng, L. He, R. Zhang and Y. Xu, Journal of Physics: Condensed Matter **31** (7), 075802 (2019).
28. S. Qiao, S. Nie, J. Zhao and X. Zhang, Applied Physics Letters **105** (17), 172406 (2014).
29. K. Lenz, E. Kosubek, K. Baberschke, H. Wende, J. Herfort, H. P. Schönherr and K. H. Ploog, Physical Review B **72** (14) (2005).
30. S. Iihama, S. Mizukami, H. Naganuma, M. Oogane, Y. Ando and T. Miyazaki, Physical Review

B **89** (17) (2014).
31. A. J. Schellekens, L. Deen, D. Wang, J. T. Kohlhepp, H. J. M. Swagten and B. Koopmans, Applied Physics Letters **102** (8), 082405 (2013).
32. S. Qiao, S. Nie, J. Zhao, Y. Huo, Y. Wu and X. Zhang, Applied Physics Letters **103** (15), 152402 (2013).

Figures

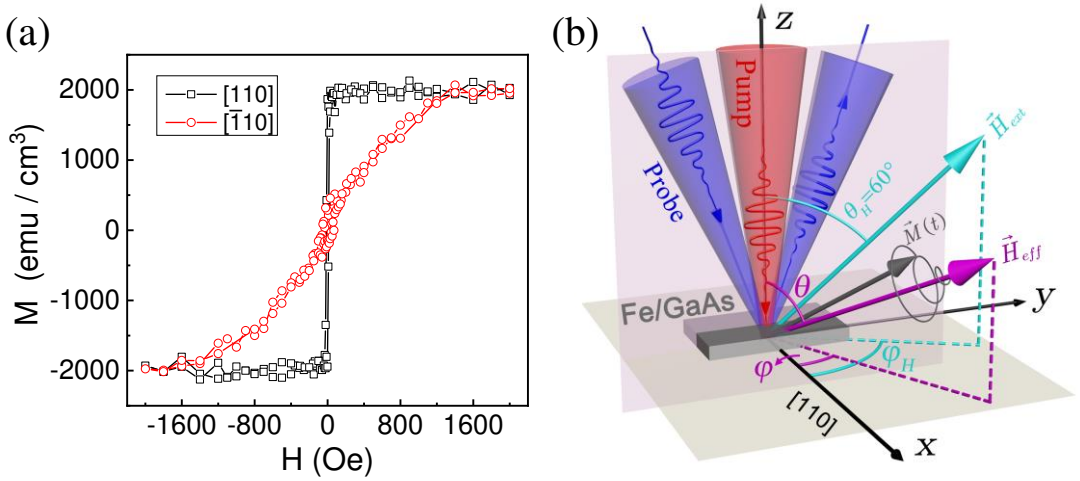

Fig. 1. (Color online) (a) The in-plane magnetic hysteresis loops of the 8 MLs Fe film along [110] (black squares) and [$\bar{1}$10] (red circles) orientations. The easy axis is along [110] orientation of the GaAs substrate. (b) Schematic geometry of the TR-MOKE measurements and the coordinate system used for the analysis.

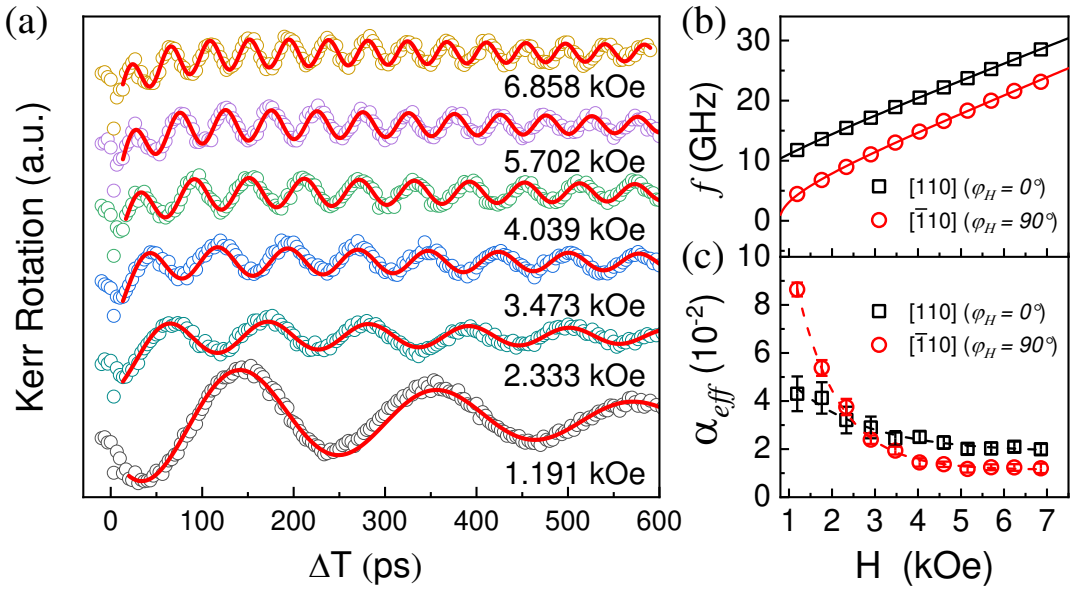

Fig. 2. (Color online) (a) Typical time-resolved Kerr rotation curves (open circles) for the 8MLs Fe film along [$\bar{1}$10] orientation (φ_H = 90°). The red solid lines are the best fitting results. The external magnetic field is applied from 1.191 kOe to 6.858 kOe, as labeled. The curves are offset for clarity. (b) The precessional frequencies as function of external magnetic field along [110] orientation (black squares) and [$\bar{1}$10] orientation (red circles). The solid lines represent the calculated results. (c) The magnetic field dependence of the effective damping factor along [110] and [$\bar{1}$10] directions. The red and black dash lines are the guides for eyes.

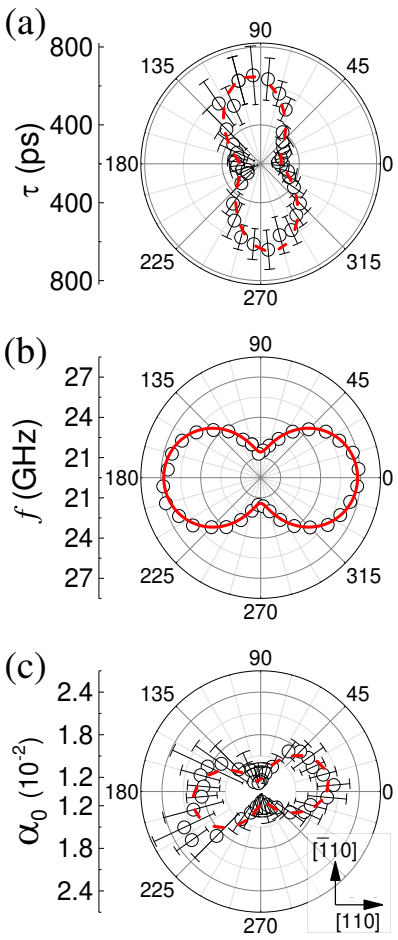

Fig. 3. Angular dependence of the (a) decay time τ, (b) frequency f, and (c) intrinsic damping constant α_0 for 8 MLs Fe film. $\varphi_H = 0°$ and $\varphi_H = 90°$ correspond to [110] and [$\bar{1}$10] orientations, respectively. The red solid line is the calculated result of frequency and the dash lines are the guides for eyes. The external field is set as 6.24 kOe to obtain α_0.

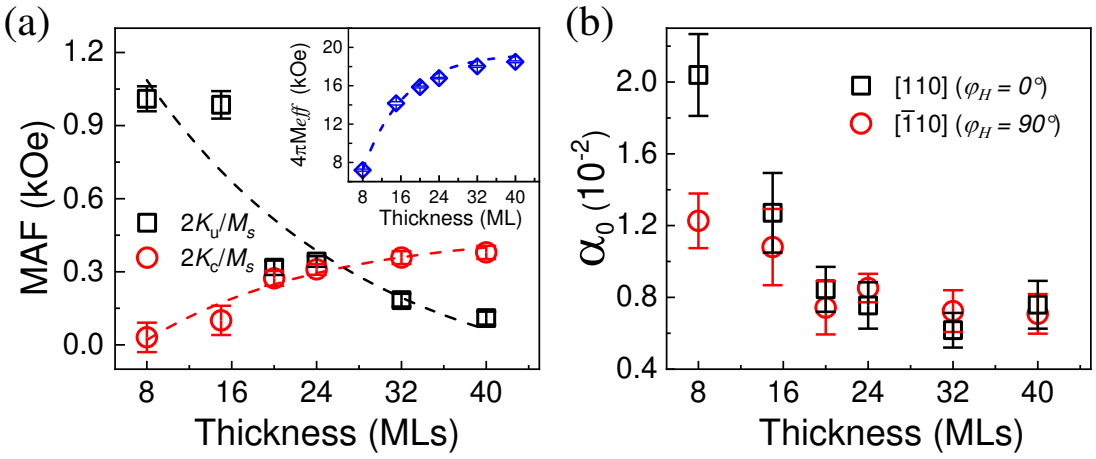

FIG. 4. (a) The magnetic anisotropy field (MAF) as a function of the thickness of Fe film. $2K_u/M_s$ (black squares), $2K_c/M_s$ (red circles), and $4\pi M_{eff}$ (blue diamonds) are magnetic uniaxial field, magnetic cubic field, and effective demagnetization field, respectively. The dash lines are the guides for eyes. (b) The intrinsic damping constant for Fe films with various thicknesses along [110] and [$\bar{1}$10] orientations, corresponding to φ_H = 0° and φ_H = 90°, respectively.